JANUARY 01 2008

A ray model for hard parallel noise barriers in high-rise cities

Kai Ming Li; Man Pun Kwok; Ming Kan Law

J. Acoust. Soc. Am. 123, 121–132 (2008)
https://doi.org/10.1121/1.2804944

A ray model for hard parallel noise barriers in high-rise cities

Kai Ming Li[a)]
Ray W. Herrick Laboratories, School of Mechanical Engineering, Purdue University, 140 South Intramural Drive, West Lafayette, Indiana 47907-2031, USA

Man Pun Kwok and Ming Kan Law
Department of Mechanical Engineering, The Hong Kong Polytechnic University, Hung Hom, Hong Kong

(Received 6 March 2007; revised 5 September 2007; accepted 11 October 2007)

A ray model is developed and validated for prediction of the insertion loss of hard parallel noise barriers placed in an urban environment either in front of a row of tall buildings or in a street canyon. The model is based on the theory of geometrical acoustics for sound diffraction at the edge of a barrier and multiple reflections by the ground, barrier and façade surfaces. It is crucial to include the diffraction and multiple reflection effects in the ray model as they play important roles in determining the overall sound pressure levels for receivers located between the façade and the near-side barrier. Comparisons of the ray model with a wave-based boundary element formulation show reasonably good agreement over a broad frequency range. Results of scale model experimental studies are also presented. It is demonstrated that the ray model agrees tolerably well with the scale model experimental data. © *2008 Acoustical Society of America.* [DOI: 10.1121/1.2804944]

PACS number(s): 43.50.Gf, 43.28.En, 43.20.Dk [KA] Pages: 121–132

I. INTRODUCTION

Construction of parallel barriers can help to attenuate noise levels on both sides of a road. Emanating from vehicles, the multiple reflections of sound waves produced by barrier surfaces create a reverberant sound field within the region of interest. These multiple reflected sound waves may travel to a receiver directly or diffract at the top edges of the parallel barriers. This phenomenon, which leads to degradation in barrier performance, is well recognized and was studied in the 1980s by Hutchins *et al.*[1–3] By assuming an incoherent nature of the source, they predicted the sound intensity levels at the top of barriers by summing the contributions from the principal wave propagation paths. Comparisons with upright and inclined parallel barriers were also made in these early studies.

It is of interest to point out that Chew[4] developed a prediction scheme for buildings situated on both sides of an expressway. Chew's model involved direct and reflected energy, both from the ground surface and multiple reflections between the parallel buildings on both sides of the expressway, and diffused energy due to scattering from the rough façade surfaces. His predictions showed that the effect of multiple reflections was significant when the distance between the buildings on opposite sides of the road was small.

Sakurai *et al.*[5] used a time-domain method to investigate the sound field of a façade-barrier system. They used a computer simulation program to evaluate the time averaging sound pressure levels in an outdoor environment. An empirical model[6] was developed to study the acoustic performance of a parallel barrier in front of a building façade. Godinho *et al.*[7] employed a boundary element formulation (BEM) to determine the shielding effects of an infinitely long barrier placed in front of tall building façades.

Despite this widespread interest, there are relatively few studies that have considered the shielding effect of parallel noise barriers in an urban environment. The prime objective of the present paper is to develop an effective numerical model to assess the acoustic performance of parallel barriers in high-rise cities. In particular, we wish to develop a numerical model to predict the sound fields in two urban scenarios: (a) when a pair of parallel barriers is flanked by a row of tall buildings, and (b) when the parallel barriers are placed in a street canyon. The numerical approach is based on the image source model developed by Li and Tang,[8] who investigated the performance of a single noise barrier in the proximity of tall buildings. The ray-based model provided accurate solutions that agreed reasonably well with indoor scaled-model experiments as well as with predictions according to the BEM formulation. On the other hand, Panneton *et al.*[9] and Muradali and Fyfe[10] used the ray model to study the acoustic performance of parallel noise barriers in the absence of other reflecting surfaces except a flat ground. The work presented in this paper is an extension of these earlier studies, but we endeavor to develop the corresponding ray model to study the acoustic performance of hard parallel barriers in high-rise cities.

This paper is organized as follows. Section II discusses the formulation of the ray model for predicting sound fields for two urban cases: (a) when a pair of parallel barriers is placed in front of a building facade, and (b) when the parallel barriers are flanked by two rows of tall buildings forming a street canyon. The image sources and image receivers are addressed in forming the ray series for computing the total sound fields. In Sec. III, we validate the ray model by comparing its predictions with those obtained by a more accurate wave-based numerical method Section IV gives the compari-

[a)]Author to whom correspondence should be addressed. Electronic mail: mmkmli@purdue.edu

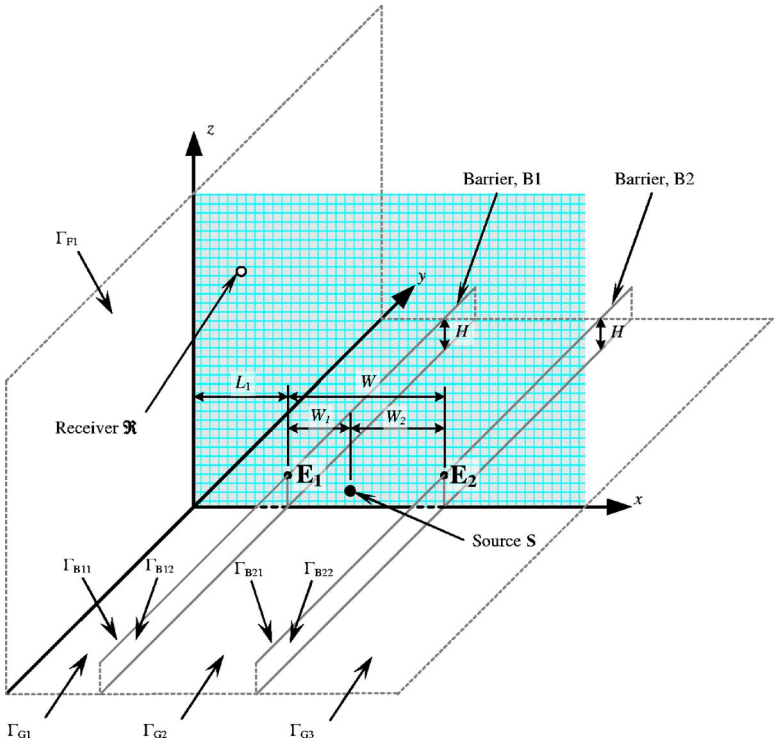

FIG. 1. (Color online) Schematic diagram of the specified problem. A source **S** is located at $\mathbf{S} \equiv (x_S, 0, z_S)$ and a receiver $\mathfrak{R}$ at $(x_R, 0, z_R)$. A pair of parallel barriers, B1 and B2 of height H is placed at a distance L_1 from a façade surface Γ_{F1} of infinite height. The barriers are separated at a distance W apart and divide the ground surface Γ_G into Γ_{G1}, Γ_{G2} and Γ_{G3}. For the configuration of a street canyon, a further façade Γ_{F2} (not shown in the diagram) is placed at a distance L_2 at the right side of B2.

sons of the ray model with indoor experimental results. Finally, a discussion and concluding remarks are discussion and concluding remarks are offered in Sec. V.

II. THEORETICAL FORMULATIONS

A. Parallel noise barriers in front of tall buildings

In the first case, we study a pair of parallel barriers placed in front of a row of tall buildings, exploring a typical urban situation in a high-rise city. Modeling this scenario, the row of tall buildings is replaced by a flat semi-infinite plane Γ_{F1} perpendicular to the ground Γ_G. To facilitate the numerical analysis, a rectangular coordinate system is chosen, where Γ_{F1} lies at the $x=0$ plane and Γ_G lies at the plane of $z=0$. The origin is located on the ground surface at the bottom of the façade. A pair of barriers is placed parallel to Γ_{F1}, where the near-side barrier B1 is located at a horizontal distance L_1 from the origin. The far-side barrier B2 is located at a horizontal distance W from B2. The distances W_1 and W_2 are, respectively, the horizontal distances measured from the source to B1 and B2. Figure 1 shows a schematic diagram of the problem considered in this case and the coordinate system used in the analysis.

We treat all boundaries in our formulation, i.e., the pair of barriers, the building façade and the ground, as made of perfectly reflecting surfaces. This assumption is justifiable as most surfaces in urban environments are acoustically hard. To simplify the analysis, we do not consider the effect of diffusion from boundary surfaces. We also limit our consideration to the following problem. The source $\mathbf{S}_0$ and receiver $\mathfrak{R}$ are located at the same vertical plane at $y=0$. The respective coordinates of the source and receiver are given by $\mathbf{S_o} \equiv (x_s, 0, z_S)$ and $\mathfrak{R} \equiv (x_R, 0, z_R)$, where $x_s \equiv (L_1 + W_1)$ and the subscripts S and R are used to represent the corresponding parameters for the source and receiver, respectively.

The pair of barriers and the building façades are infinitely long and aligned along the y axis. With these assumptions, the contributions from the top edge of the façade and the vertical edges at the ends of the barriers are excluded from our analysis. Parallel barriers, which are used to shield traffic noise in high-rise cities, are built to the same height in most practical situations. Therefore, we only consider the case when they have the same height, $H \geqslant z_s$. It is straightforward to extend the current work to study the pair of barriers, B1 and B2, with different heights. We point out that the top edges of B1 and B2 are denoted by $\mathbf{E1} \equiv (L_1, y, H)$ and $\mathbf{E2} \equiv (L_1 + W, y, H)$, respectively.

B. Image source model

As the source $\mathbf{S}_0$ is placed between the parallel surfaces, a row of image sources are formed as follows. An image source $\mathbf{S}_{-1}$ is created because of the reflection of the source $\mathbf{S}_0 (\equiv \mathbf{S}_1)$ on the surface of B1. Image sources $\mathbf{S}_2$ and $\mathbf{S}_3$ are then formed because of the reflection of the image sources $\mathbf{S}_1$ and $\mathbf{S}_{-1}$ on the surface of B2. Next, image sources $\mathbf{S}_{-2}$ and $\mathbf{S}_{-3}$ are created, and so on, see Fig. 2. We see that a series of image sources $\mathbf{S}_1$, $\mathbf{S}_2$, $\mathbf{S}_3, \ldots$ is generated to the right side of B1. The image source $\mathbf{S}_2$ creates the ray that hits B2 before it reaches the receiver $\mathfrak{R}$. The image source $\mathbf{S}_3$ is formed for the ray that hits B1 and then B2 before it reaches $\mathfrak{R}$. The procedure continues for determining the ray paths traced by other image sources, $\mathbf{S}_3$, $\mathbf{S}_4$, and so on. Similarly, image sources $\mathbf{S}_0$, $\mathbf{S}_{-1}$, $\mathbf{S}_{-2}$, etc., are constructed at the left side of B2. We note here that the image source $\mathbf{S}_0 (\equiv \mathbf{S}_1)$ is the source itself. It is included in this series for facilitating notations used in the subsequent analysis. Image source $\mathbf{S_{-1}}$ produces a ray that hits B1 before it reaches $\mathfrak{R}$. Image source $\mathbf{S_{-2}}$ generates the ray that hits B2 and then B1 before arriving at $\mathfrak{R}$. Again, image sources $\mathbf{S_{-3}}$, $\mathbf{S_{-4}}$, and so on are

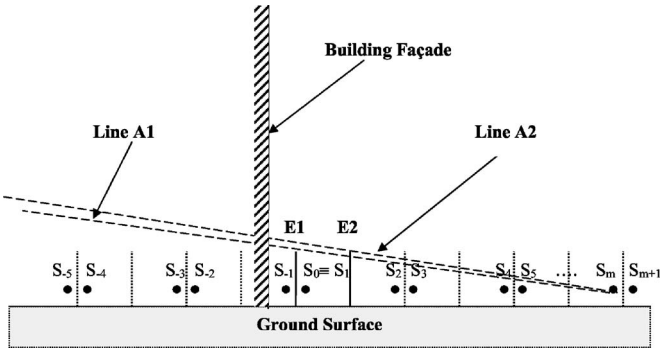

FIG. 2. Schematic diagram of the image sources $\mathbf{S}_{\pm}$ formed on reflections from the pair of parallel barriers. Lines A1 and A2 are drawn, forming a region where an image source $\mathbf{S_m}$ can reach an image receiver. E1 and E2 are the respective edges of the near-side and far-side barriers. A receiver is located in the illumination zone due to the image source S_{m} if it lies above Line A2. It is situated in the penumbra region if the receiver is located between Lines A1 and A2. If the receiver stays below Line A1, then it is located in the shadow zone.

formed in an analogous manner. For convenience, we denote these as $(\mathbf{S_0},\mathbf{S_{-1}},\mathbf{S_{-2}},\ldots)\in\mathbf{S}_-$ and $(\mathbf{S_1},\mathbf{S_2},\mathbf{S_3},\ldots)\in\mathbf{S}_+$.

There are two analogous series of image sources $(\mathbf{\Lambda_{-1}},\mathbf{\Lambda_{-2}},\mathbf{\Lambda_{-3}},\ldots)\in\mathbf{\Lambda}_-$ and $(\mathbf{\Lambda_1},\mathbf{\Lambda_2},\mathbf{\Lambda_3},\ldots)\in\mathbf{\Lambda}_+$ that can also be identified because of the presence of a reflecting ground. These ground reflected image sources are not shown in Fig. 2 for reasons of clarity. The rays of these image sources hit the ground once before they reach $\mathfrak{R}$. The locations of these image sources, $\mathbf{S}_{\pm m}=(x_{\pm m},0,z_s)$ and $\mathbf{\Lambda}_{\pm m}=(x_{\pm m},0,-z_s)$, can be determined from the geometrical configuration of the problem, where the x coordinates of these image sources are given by

$$x_{\pm m}=L_1\pm(mW-W_{(m)})\quad\text{for } m=1,2,3,\ldots, \tag{1a}$$

where

$$W_{(m)}=\begin{cases}W_2 & \text{if } m \text{ is odd}\\ W_1 & \text{if } m \text{ is even}\end{cases} \tag{1b}$$

and $x_0=x_1$. For the image source method, the total sound field at a particular receiver location is a coherent summation of contributions from all these image sources. The main task, however, is to identify all the possible image sources and calculate the corresponding contributions.

A possible sound ray from an image source is determined by establishing a valid transmission path linking the source and receiver. These possible ray paths may be obtained through direct transmission, reflections from the boundary surfaces, and diffractions at the top edge of the barrier. They can also be any combination of reflections and diffractions with different orders. In summary, the total sound field is given by

$$p(\mathbf{S},\mathfrak{R})=P_{\mathrm{direct}}+P_{\mathrm{diffract}}, \tag{2}$$

where P_{direct} takes into account for both direct transmission and the reflections from the boundary surfaces from the source to receiver. The term, P_{diffract}, is the total contributions from the diffracted ray paths. To reduce the complexity in the determination of all possible ray paths, we only consider the diffraction terms with the first order. Any higher order terms are ignored.[9,10] This assumption is justifiable because the contributions from the diffracted sound waves are generally much less than from the direct and reflected waves. By this simplification, the contributions can be classified into primary and secondary groups in the following sections.

C. Illumination zone

The primary group of contributions is generated by image sources where they can be "viewed" by the receiver $\mathfrak{R}$ in a direct line of sight, i.e., the effect of the diffraction at the barrier edges does not play a role in calculating the sound field. The ray paths in this group are established either as a direct transmission or multiple reflections from boundary surfaces.

We are interested in the situation when the receiver is located behind the near-side barrier but in front of the façade, i.e., $0\leqslant x_R\leqslant L_1$ and $z_R\geqslant 0$. With these restrictions, only image sources $\mathbf{S}_m$ and $\mathbf{\Lambda}_m$ (for a positive integral value of m), located at the right side of B1, may "see" the receiver directly. Since the parallel barriers have a finite height of H, further conditions are needed in order to determine whether a ray emanating from image sources $\mathbf{S}_m$ or $\mathbf{\Lambda}_m$ can reach a receiver. This is because the surface of B1 may be too high to shield a direct sight-line contact, and B2 may be too low to provide a surface for the reflection of an incoming ray. By extending a line A_1 joining $\mathbf{S}_m$ to **E1**, and another line A_2 linking $\mathbf{S}_m$ and **E2**, see Fig. 2, we can determine the limit of the regions where the ray path from $\mathbf{S}_m$ can reach the receiver. We can classify that the receiver is situated in the illumination zone due to the image source, S_m if it is located above Line A2. The receiver is positioned in the penumbra region if it is located between Line A1 and A2. Finally, the receiver lies in the shadow zone if it is placed below Line A1.

Because of the reflection from the buildings, additional ray paths can also be constructed for the situation when the sound rays hit the façade surface before reaching the receiver. In this case, it is convenient to consider the reception point consisting of a pair of the image receivers, $\mathfrak{R}_{\pm1}\equiv(\pm x_{\mathrm{R}},0,z_{\mathrm{R}})$, where $\mathfrak{R}_1$ corresponds to the direct arrival of a sound ray and $\mathfrak{R}_{-1}$ is the reflection of sound from the façade. With the introduction of $\mathfrak{R}_{\pm1}$, all possible ray paths can be found by connecting $\mathbf{S}_m$ or $\mathbf{\Lambda}_m$ to $\mathfrak{R}_{\pm1}$. The presence of $\mathbf{S}_m$ in the total sound field can be determined by extending the lines joining $\mathbf{S}_m$ and $\mathfrak{R}_{\pm1}$ to yield the following additional condition:

$$\frac{(z_s-H)(\pm x_R-L_1-W)}{(m-1)W-W_{(m)}}\geqslant z_R-H\geqslant\frac{(z_s-H)(\pm x_R-L_1)}{mW-W_{(m)}}, \tag{3}$$

where $W_{(m)}$ is given in Eq. (1b). These two conditions correspond respectively to lines A_1 and A_2 as shown in Fig. 2. Similarly, the condition for the presence of $\mathbf{\Lambda}_m$ in the ray series can be determined as follows:

$$\frac{(H+z_s)(\pm x_R - L_1 - W)}{W_{(m)} - (m-1)W} \geqslant z_R - H \geqslant \frac{(H+z_s)(\pm x_R - L_1)}{W_{(m)} - mW}. \tag{4}$$

In Eqs. (3) and (4), a positive sign for x_R represents the condition for the receiver $\mathfrak{R}_1$, and a negative sign gives the corresponding condition for the image receiver $\mathfrak{R}_{-1}$.

We remark that there is no primary contribution of the total sound fields when the receiver is located in the shadow zone when $z_R \leqslant H$. The sound field from the primary group can be obtained by summing all possible contributions

$$P_{\text{direct}} = \sum_{m=m_<}^{m_>} G_d(\mathbf{S_m}, \mathfrak{R}_{\pm 1}) + \sum_{m=m_<}^{m_>} G_d(\mathbf{\Lambda_m}, \mathfrak{R}_{\pm 1}). \tag{5}$$

In the above equation, $\mathfrak{R}_1$ and $\mathfrak{R}_{-1}$ are substituted, in turn, obtaining four separate series. The term $\mathfrak{R}_1$ corresponds to the rays linking the image sources to the receiver, and $\mathfrak{R}_{-1}$ represents the contributions of those rays that have an extra reflection from the building façade before they reach the receiver. For a given source and receiver position, a range of m (from m_1 to m_2, say) can be determined from Eqs. (3) and (4). For instance, this information can be obtained for $\mathbf{S}_1$ and $\mathfrak{R}_1$ from Eq. (3) with the positive sign taken. We can see that $m_<$ and $m_>$ are given by

$$m_< = \min(m_1, m_2), \tag{6a}$$

$$m_> = \max(m_3, m_4), \tag{6b}$$

where m_1 is the smallest odd integer just greater than $W_2/W + (H+z_s)(x_R - L_1)/[W(z_R - H)]$, m_2 is the smallest even integer just greater than $W_1/W + (H+z_s)(x_R - L_1)/[W(z_R - H)]$, m_3 is the largest odd integer just smaller than $W_2/W + (z_s - H)(x_R - L_1 - W)/[W(z_R - H)] + 1$, and m_4 is the largest even integer just smaller than $W_1/W + (z_s - H)(x_R - L_1 - W)/[W(z_R - H)] + 1$.

Different ray paths have different $m_<$ and $m_>$ but they can be determined straightforwardly from the corresponding conditions given in Eqs. (3) and (4). For example, suppose that we have the source located at $\mathbf{S}_1 = (7.5, 0, 0.25)$, the near-side barrier is located at $L_1 = 5$ m from the façade, the parallel barrier has a height $H = 2.5$ m, the source is located at $W_1 = 2.5$ m from the near-side barrier, and $W_2 = 7.5$ m from the far-side barrier. If the receiver is located in the illumination zone at $\mathfrak{R} \equiv \mathfrak{R}_1 = (1.0, 0, 10)$, then we can determine that $m_>$ and $m_<$ are all equal to 1 for all series given in the summation of Eq. (5). In other words, only $\mathbf{S}_1$ and $\mathbf{\Lambda}_1$ can see the image receivers, $\mathfrak{R}_{\pm 1}$. On the other hand, if the receiver is located at a lower height at $\mathfrak{R} \equiv \mathfrak{R}_1 = (1.0, 0, 3.5)$, then we can show that the image sources $\mathbf{S_2} - \mathbf{S_5}$ and $\mathbf{\Lambda_2} - \mathbf{\Lambda_5}$ can see $\mathfrak{R}_{-1}$, but only the image sources $\mathbf{S_2} - \mathbf{S_4}$ and $\mathbf{\Lambda_2} - \mathbf{\Lambda_5}$ can see $\mathfrak{R}_1$. We only sum the contributions from those terms that can establish a sight-line contact between the image sources and image receivers in the series of Eq. (5).

In general, the Green function $G_d(\mathbf{S}, \mathbf{R})$ stands for the sound field radiated directly from an arbitrary point source $\mathbf{S}$ to any reception point $\mathbf{R}$. It is computed by

$$G_d(\mathbf{S}, \mathbf{R}) = \exp(ikd)/4\pi d, \tag{7}$$

where d is the direct distance measured from the source $\mathbf{S}$ to the receiver $\mathbf{R}$. Equations (3) and (4) are applied to ensure a possible direct link between $\mathbf{S}$ and $\mathbf{R}$. No contribution from a particular image source is possible if the corresponding conditions are not satisfied. Nevertheless, only a finite number of rays is summed in Eq. (5), and contributions from image sources located at long distances from the receiver and its image are truncated because of reduced sound levels due to the effect of geometrical spreading of the sound rays.

Next, we wish to discuss the secondary group of contributions. This group of rays consists of diffractions from the edges of the parallel barriers. We reiterate that the higher order diffraction terms are generally ignored in the present analysis, but there may be various orders of reflections both before and after the diffraction at the barrier edges, $(\mathbf{E1}, \mathbf{E2}) \in \mathbf{E}$. We may treat $\mathbf{E}$ as virtual receivers that can be viewed by the image sources. At the source side of the barrier, multiple reflections can then be handled effectively by connecting image sources to $\mathbf{E}$. We shall denote these image sources by $\mathbf{S}_{\pm n}$ and $\mathbf{\Lambda}_{\pm n}$ although, strictly speaking, they are the same image sources situated at the same locations as $\mathbf{S}_{\pm m}$ and $\mathbf{\Lambda}_{\pm m}$ if $m = n$. For clarity, different subscripts are chosen to distinguish the ray paths traced by the same image sources for the direct (the subscript m is used) and diffracted (the subscript n is used) fields.

To handle the multiple reflections at the receiver side of the barrier, we find it convenient to introduce the concept of the image receiver, because E1 and E2 can be seen as two secondary sources from the receiver location. On this side of the barrier, multiple reflections can be established when the sound rays leave $\mathbf{E}$ and hit the outer surface of the near-side barrier and the façade surface before they reach the receiver. The ray paths originating from the barrier edges can then be determined easily by linking $\mathbf{E}$ with the receiver and its images.

If $z_R > H$, there are only two image receivers – the receiver $\mathfrak{R}_1$ and its image $\mathfrak{R}_{-1}$. These locations were discussed in the preceding paragraphs when we addressed the contributions of direct waves from the image sources. Both barrier edges, $\mathbf{E}_1$ and $\mathbf{E}_2$, can see $\mathfrak{R}_{\pm 1}$. The image sources on the right side of B1, $\mathbf{S}_n$ and $\mathbf{\Lambda}_n$, can see $\mathbf{E}_1$. On the other hand, only the image sources on the left side of B2, $\mathbf{S}_-$ and $\mathbf{\Lambda}_-$ can see $\mathbf{E}_2$. In addition to these image receivers, we can also identify another pair of image receivers, $\Psi_{\pm 1}$, because of the presence of the reflecting ground between Γ_{F1} and B1. Only the edge of the near-side barrier, $\mathbf{E1}$, can see $\Psi_{\pm 1}$. The surface of B1 shields the sound rays connecting E2 to $\Psi_{\pm 1}$. The total diffracted field in this region, $z_R > H$ and $L_1 > x_R > 0$, can then be written as

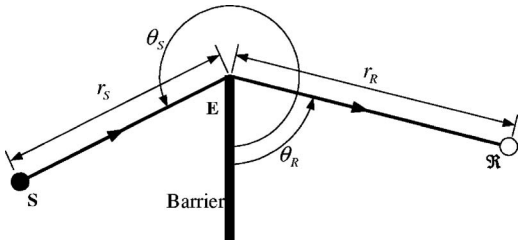

FIG. 3. Schematic diagram of the geometrical configuration for the diffraction of sound by a thin barrier.

$$P_{\text{diffract}} = \sum_{n=1}^{\infty} [G_f(\mathbf{S_n}, \mathfrak{R}_{\pm 1}|\mathbf{E_1}) + G_f(\mathbf{\Lambda_n}, \mathfrak{R}_{\pm 1}|\mathbf{E_1})] + \sum_{n=1}^{\infty} [G_f(\mathbf{S_n}, \mathbf{\Psi}_{\pm 1}|\mathbf{E_1}) + G_f(\mathbf{\Lambda_n}, \mathbf{\Psi}_{\pm 1}|\mathbf{E_1})] + \sum_{n=0}^{\infty} [G_f(\mathbf{S_{-n}}, \mathfrak{R}_{\pm 1}|\mathbf{E_2}) + G_f(\mathbf{\Lambda_{-n}}, \mathfrak{R}_{\pm 1}|\mathbf{E_2})], \tag{8}$$

where $\mathfrak{R}_1$, $\mathfrak{R}_{-1}$, $\mathbf{\Psi}_1$ and $\mathbf{\Psi}_{-1}$ are substituted in turn. We remark that the third series starts with $n=0$ accounting for the ray path that reaches **E2** directly from image sources $\mathbf{S}_0(\equiv\mathbf{S_1})$ and $\mathbf{\Lambda}_0(\equiv\mathbf{\Lambda}_1)$. The Green function $G_f(\mathbf{S},\mathfrak{R}|\mathbf{E})$ is the solution for sound diffracted by a hard noise barrier with edge **E** for a source **S** and receiver $\mathfrak{R}$. It is given by[11]

$$G_f(\mathbf{S},\mathfrak{R}|\mathbf{E}) = \left(\frac{e^{i\pi/4}}{\sqrt{2}}\right)\left[\frac{e^{ik(d_S+d_R)}}{4\pi(d_S+d_R)}\right][A_D(X_+) + A_D(X_-)], \tag{9}$$

where d_S and d_R are the respective distances from the source and receiver to the diffraction point. The function, $A_D(X)$ is the diffraction integral[11] given by

$$A_D(X) = \text{sgn}(X)[f(|X|) - ig(|X|)], \tag{10}$$

where sgn(X) is the sign function, and $f(X)$ and $g(X)$ are the auxiliary Fresnel functions[12] of real argument X. The arguments of the diffraction integral, X_+ and X_-, are determined by

$$X_\pm = X(\phi_R \pm \phi_S), \tag{11a}$$

where

$$X(\Phi) = \left[-2\cos\left(\frac{\Phi}{2}\right)\right]\sqrt{\frac{2\cdot d_S\cdot d_R}{\lambda(d_S+d_R)}}, \tag{11b}$$

λ is the wavelength of the diffracted sound, and the angles ϕ_R and ϕ_S are defined in the surface of the screen as shown in Fig. 3. The argument Φ in Eq. (11b) is $(\phi_R \pm \phi_S)$ for $X_\pm$.

D. Shadow zone

The receiver is located at the shadow zone if $z_R \leqslant H$. In this case, the façade and the outer face of B1 form a pair of reflecting surfaces. It is possible to generate a row of image receivers, $(\mathfrak{R}_{-j}, \mathfrak{R}_j) \in \mathfrak{R}$. The positions of these image receivers, $\mathfrak{R}_{\pm j} \equiv (\xi_{\pm j}, 0, z_R)$ for $j=1,2,3,\ldots$, can be determined readily to give

$$\xi_{\pm j} = \pm jL_1 - D_{(j)}, \tag{12}$$

where

$$D_{(j)} = \begin{cases} x'_R & \text{if } q \text{ is odd} \\ x_R & \text{if } q \text{ is even} \end{cases} \tag{13}$$

and $x'_R(\equiv L_1 - x_R)$ is the horizontal distance of the receiver position measured from B1.

Only those image receivers situated on the left side of B1, …, $\mathfrak{R}_{-3}, \mathfrak{R}_{-2}, \mathfrak{R}_{-1}$ and the receiver $\mathfrak{R}_0 \equiv \mathfrak{R}_1$ itself, can see $\mathbf{E}_1$. Image receiver $\mathfrak{R}_{-1}$ traces the following sound ray: leaves $\mathbf{E}_1$, hits the building façade and arrives at the receiver. Image receiver $\mathfrak{R}_{-2}$ follows the ray path: leaves $\mathbf{E}_1$, hits the building façade, the outer face of B1 and arrives at the receiver. This process repeats for other image receivers $\mathfrak{R}_{-3}, \mathfrak{R}_{-4}, \ldots$ and so on. Since there is a reflecting ground between Γ_{F1} and B1, another row of image receivers, $\mathbf{\Psi}_{\pm j} \equiv (\xi_{\pm j}, 0, -z_R)$ for $j=1,2,3,\ldots$, is formed with $\xi_{\pm j}$ given by Eq. (12). Again, only the image sources $\mathbf{\Lambda}_n$ (for $n=1,2,3$) can see **E1**. It is worth noting that **E2** can see none of these image receivers in the region $z_R < H$ and $L_1 > x_r > 0$, because the near side barrier B1 prevents any contact without a further diffraction at its edge. Hence the total diffracted field is simply

$$P_{\text{diffract}} = \sum_{n=1}^{\infty}\sum_{j=0}^{\infty} [G_f(\mathbf{S_n}, \mathfrak{R}_{-j}|\mathbf{E1}) + G_f(\mathbf{\Lambda_n}, \mathfrak{R}_{-j}|\mathbf{E1})] + \sum_{n=1}^{\infty}\sum_{j=0}^{\infty} [G_f(\mathbf{S_n}, \mathbf{\Psi}_{-j}|\mathbf{E1}) + G_f(\mathbf{\Lambda_n}, \mathbf{\Psi}_{-j}|\mathbf{E1})], \tag{14}$$

where the inner series for the index j starts from 0 to include the terms for the rays connecting from E1 to the receiver and its image on reflection from the ground surface. Again, the Green function $G_f(\mathbf{S},\mathbf{R}|\mathbf{E})$ represents the solution for the diffracted sound field. The diffracted terms are calculated for different combinations of image sources, n and image receivers, j. We also take $\mathfrak{R}_0 \equiv \mathfrak{R}_1$ and $\mathbf{\Psi}_0 = \mathbf{\Psi}_1$ in writing a more compact series given in Eq. (14).

E. Parallel barriers in a street canyon

In the second case, we consider that the pair of parallel barriers, B1 and B2, is placed in a street lined with two parallel rows of tall buildings. The tall buildings are replaced by two flat façade surfaces, Γ_{F1} and Γ_{F2}, perpendicular to the ground. The geometrical configuration of this problem is similar to that described in Sec. II. Again, the separation between the pair of barriers is W and the source is located at W_1 from B1 and W_2 from the far-side barrier B2. The near-side barrier B1 is situated at a distance of L_1 from Γ_{F1}, and B2 is located at a distance of L_2 from Γ_{F2}. The second case is a relatively more complicated problem than the first because of the presence of the additional façade forming the so-called street canyon. However, the total sound field is computed according to Eq. (2) with different P_{direct} and P_{diffract} from those derived in the last section.

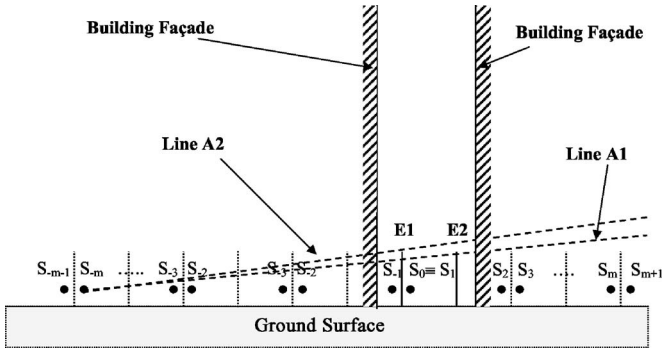

FIG. 4. Schematic diagram of the image sources $\mathbf{S}_{\pm}$ formed on reflections from the pair of parallel barriers. Lines A1 and A2 are drawn, forming a region where an image source $\mathbf{S}_{-\mathbf{m}}$ can reach an image receiver. E1 and E2 are the respective edges of the near-side and far-side barriers. A receiver is located in the illumination zone due to the image source $\mathbf{S}_{-\mathrm{m}}$ if it lies above Line A2. It is situated in the penumbra region if the receiver is located between Lines A1 and A2. If the receiver stays below Line A1, then it is located in the shadow zone.

From the modeling point of view, this problem is the same as the case described in Sec. II A. The only exception is that a further façade surface, Γ_{F2}, is added at the right side of B2. Indeed, when the source is placed at $z_s < H$, and the receiver is located in the region $0 \leqslant x_R \leqslant L_1$ and $z_R \leqslant H$, the sound field in the shadow zone is the same as the first case provided that higher order diffraction terms are ignored. Hence, our focus in this section is the determination of the sound field in the illumination zone.

In this region, where $0 \leqslant x_R \leqslant L_1$ and $z_R > H$, we can again identify a row of image receivers $[(\mathfrak{R}_{-j}, \mathfrak{R}_j) \in \mathfrak{R}$ for $j=1,2,3,\ldots]$ due to the presence of Γ_{F1} and Γ_{F2}. These image receivers are located at $\mathfrak{R}_{\pm j} \equiv (\xi_{\pm j}, 0, z_R)$, with $\xi_{\pm j}$ given by

$$\xi_{\pm j} = \pm j(L_1 + L_2 + W) - D_{(j)}, \tag{15}$$

where

$$D_{(j)} = \begin{cases} \bar{x}_R & \text{if } j \text{ is odd} \\ x_R & \text{if } j \text{ is even} \end{cases}, \tag{16}$$

and $\bar{x}_R$ is the horizontal distance of the receiver position measured from Γ_{F2}, i.e., $\bar{x}_R = L_1 + L_2 + W - x_R$.

The primary group of contributions can be determined by identifying the series of image sources and image receivers that can see each other. The image sources on the right side of B1, i.e. $(\mathbf{S}_m, \mathbf{\Lambda}_m) \in \mathbf{S}_+$, can see the image receivers $\mathfrak{R}_{-j} \in \mathfrak{R}_-$ located on the left side of Γ_{F2}. The additional conditions for establishing these sight lines are given in the analog forms as Eqs. (3) and (4), except that $\pm x_{\mathrm{R}}$ in these two equations is replaced by ξ_{-j} for $j=0,1,2,\ldots$, in turn. Similarly, the image sources located on the left side of B2, $(\mathbf{S}_{-m}, \mathbf{\Lambda}_{-m}) \in \mathbf{S}_-$, can view the image receivers $\mathfrak{R}_j \in \mathfrak{R}_+$ situated on the right side of Γ_{F2}. By considering Fig. 4, the additional conditions for the image sources $\mathbf{S}_{-m}$ and Λ_{-m} are determined, respectively, as follows:

$$\frac{(z_s - H)(\xi_j - L_1)}{mW - W_{(m)}} \geqslant z_R - H \geqslant \frac{(z_s - H)(\xi_j - L_1 - W)}{(m+1)W - W_{(m)}} \tag{17}$$

and

$$\frac{(z_s + H)(\xi_j - L_1)}{mW - W_{(m)}} \geqslant z_R - H \geqslant \frac{(z_s + H)(\xi_j - L_1 - W)}{(m+1)W - W_{(m)}}. \tag{18}$$

We can also determine the ranges of m $[m_1(j)$ and $m_2(j)]$ for different values of j. With this information, we can express immediately the contribution of the total field from this group of image sources as a double summation of direct fields from a combination of image sources $\mathbf{S}_{\pm}$ of the index m to the image receivers $\mathfrak{R}_{\pm}$ of the index j:

$$\begin{aligned} P_{\mathrm{direct}} = & \sum_{j=0}^{\infty} \sum_{m=m_<(j)}^{m_>(j)} G_d(\mathbf{S}_m, \mathfrak{R}_{-j}) + \sum_{j=0}^{\infty} \sum_{m=m_1(j)}^{m_>(j)} G_d(\mathbf{\Lambda}_m, \mathfrak{R}_{-j}) \\ & + \sum_{j=1}^{\infty} \sum_{m=m_<(j)}^{m_>(j)} G_d(\mathbf{S}_{-m}, \mathfrak{R}_j) \\ & + \sum_{j=1}^{\infty} \sum_{m=m_<(j)}^{m_2(j)} G_d(\mathbf{\Lambda}_{-m}, \mathfrak{R}_j). \end{aligned} \tag{19}$$

The first two series start at $j=0$ to include the receiver in the row of image receivers $\mathfrak{R}_-$. The existence of a particular ray path is determined by satisfying the corresponding conditions given in Eqs. (17) and (18). The Green function G_d of the direct field given above can be calculated according to Eq. (7).

The contribution of the diffracted field can also be expressed in a rather similar form except that the pair of receivers $\mathbf{R}_{\pm 1}$ in Eq. (8) is replaced by a series of $\mathfrak{R}_{\pm j}$for $j=1,2,3,\ldots$. An additional sum is needed for the contributions from each of the image sources to each of the image receivers as follows:

$$\begin{aligned} P_{\mathrm{diffract}} = & \sum_{j=1}^{\infty} \sum_{n=1}^{\infty} [G_f(\mathbf{S_n}, \mathfrak{R}_{\pm j} | \mathbf{E_1}) + G_f(\mathbf{\Lambda_n}, \mathfrak{R}_{\pm j} | \mathbf{E_1})] \\ & + \sum_{j=0}^{\infty} \sum_{n=1}^{\infty} [G_f(\mathbf{S_n}, \mathbf{\Psi}_{-j} | \mathbf{E_1}) + G_f(\mathbf{\Lambda_n}, \mathbf{\Psi}_{-j} | \mathbf{E_1})] \\ & + \sum_{j=1}^{\infty} \sum_{n=0}^{\infty} [G_f(\mathbf{S_n}, \mathfrak{R}_{\pm j} | \mathbf{E_2}) + G_f(\mathbf{\Lambda_n}, \mathfrak{R}_{\pm j} | \mathbf{E_2})], \end{aligned} \tag{20}$$

where $G_f(\mathbf{S}, \mathbf{R} | \mathbf{E})$ is the Green function for the diffraction of sound from a source $\mathbf{S}$ to a receiver $\mathbf{R}$ at an edge $\mathbf{E}$. In Eq. (20), the term involving $\mathfrak{R}_{\pm j}$ is substituted with $\mathfrak{R}_j$ and $\mathfrak{R}_{-j}$ in turn. The second ray series of the above equation starts from $j=0$ and includes the image receiver $\mathbf{\Psi}_0 (\equiv \mathbf{\Psi}_1)$.

III. NUMERICAL COMPUTATIONS

The ray (image source) model provides an effective and efficient methodology to assess the acoustic performance of parallel barriers in front of a tall building. Our approach is a direct extension of the earlier developments. In the absence of a building façade, our model is analogous to the prediction methods for parallel barriers proposed by Panneton *et al.*[9] and Muradali.[10] Without the far side barrier, our model is identical to that proposed by Li and Tang[8] for predicting the

acoustic performance of a single barrier placed in front of a building façade. Prior numerical analyses were conducted to compare our model with the published simulation data.[8–10] These comparison results, which show good agreement, serve to confirm the validity of our numerical model and they are not shown here for succinctness.

Next, the numerical results predicted by the image source model are compared with that evaluated by a wave-based numerical formulation. As the geometrical configuration of the present study is an external problem, the boundary element method (BEM) is an appropriate approach for the purpose of validation. In fact, the BEM formulation has been extensively used to study the physical phenomenon of outdoor sound propagation in an irregular terrain and to study the acoustic performance of noise barriers. In the present study, the height of the building façade is taken as 25 m, which should be sufficiently tall to ensure that any contributions due to the diffraction of the sound at the façade's top edge are negligibly small. Generally speaking, more elements are needed at higher frequencies in order to represent the boundary surfaces. They are partitioned with at least ten elements per wavelength in the present study. This requirement ensures a higher degree of accuracy for the numerical results.

A realistic outdoor configuration is used in our analysis. The near-side and far-side barriers, B1 and B2, have identical heights of 2.5 m, and are situated at 5 and 15 m in front of building façade Γ_{F1}, respectively. A further parallel building façade, Γ_{F2}, is placed 20 m from Γ_{F1} in the case of street canyons. In both cases, an omni-directional noise source is located between the parallel barriers at 0.25 m above the ground and 7.5 m in front of the façade, Γ_{F1}. In other words, the source is located 2.5 m from B1 and 12.5 m from B2. The reception points are chosen at 1 m away from Γ_{F1} and with different heights above the ground for the presentation of the numerical results. The choice of these source/receiver geometries allows our numerical models to examine the sound fields in different areas of interest—shadow, penumbra and illumination zones, respectively.

It is of interest to point out that the BEM formulation generally requires relatively higher computational resources especially at high frequencies. To put it in context, let us consider a critical example with a source operating at 5 kHz. These are the highest frequencies we showed in the numerical simulations using the BEM formulations. A FORTRAN program was used to compute the sound field for a pair of parallel barriers locating in a street canyon. A total in excess of 9000 boundary elements (about 3800 for each façade surface and 750 for each barrier) are needed in this case. It took over 30 h for a typical desktop computer (a 2 GHz processor and 1 Giga bytes of RAM memory) to solve the set of simultaneous equations by using a standard matrix method. The computational time for the BEM formulation will increase exponentially for the source frequency extending beyond 5 kHz and for the façade surfaces reaching higher than 25 m. On the other hand, we have developed a suite of MATLAB program for the image source model. The MATLAB program was compiled and was used to predict the sound fields for the two urban scenarios as described in the earlier sections. Using the same desktop computer, the computational time was about 10 min for a source frequency of 5 kHz. It took nearly the same time to compute the sound fields for all other frequencies of interests. The computational time can be reduced further if a FORTRAN program was developed and used to predict the sound fields by the image source model. However, there is no attempt to follow along this route for minimizing the computational time in the present study.

We note that relatively less image sources are required if the receiver is situated in the shadow zone close to the ground. In this situation, only a few reflections from the boundary surfaces are normally required to obtain a set of converged numerical results. On the other hand, more image sources are needed if the receiver is located higher above the ground in the penumbra region and the illumination zone. Although it is possible to optimize the number of image sources required for different receiver heights, we find that variations in the sound pressure level generally become stable after about 60 reflections over 1/3 octave bands varying from 125 Hz to 8 kHz. For simplicity, we set the maximum orders of reflections to be no more than 100 for both sides of the barriers at all receiver locations. This will lead to a simpler program with an acceptable numerical accuracy at the expense of a modest increase in the overall computational time.

Four receiver locations are chosen for comparison in these two cases—parallel barriers in front of building facades and in a street canyon. For the first two locations, Locations 1 and 2, the receiver $\mathfrak{R}$ is placed at points (1, 0, 1) and (1, 0, 2), respectively. Both of these locations are situated in the shadow zone of B1. In Location 3, the receiver $\mathfrak{R}$ is placed at (1, 0, 5) which is close to the direct line of sight of E1 in the penumbra region. The receiver, which is positioned at $\mathfrak{R}=(1,0,10)$, is illuminated directly by the source in Location 4.

We introduce a term known as the insertion loss (*IL*) to facilitate the presentation of the numerical results. It is defined as follows:

$$IL = 20\log_{10}\left(\frac{P_w}{P_{w/o}}\right), \tag{21}$$

which is essentially the difference in sound pressure levels before and after the installation of parallel barriers. Figures 5 and 6 show the predicted *IL* spectra at Locations 1 and 3 for the pair of parallel barriers placed in front of the façade surface. The general trend of the *IL* spectra such as the positions of the peaks and dips predicted by the image source method coincides well with those predicted by the BEM formulation. Although there are noticeable discrepancies for the predicted magnitudes at some frequencies between these two methods, these differences will be less significant if the results are averaged over a frequency band. The comparison of *IL* spectra in 1/3 octave bands will be shown in the next section. It is remarkable as shown in Figs. 5 and 6 that there is a higher level of fluctuation in *IL* at high frequencies as predicted by both methods. This can be explained by using the image source method as follows. The total sound field is computed by summing the contributions coherently from a finite number of image sources produced by multiple reflec-

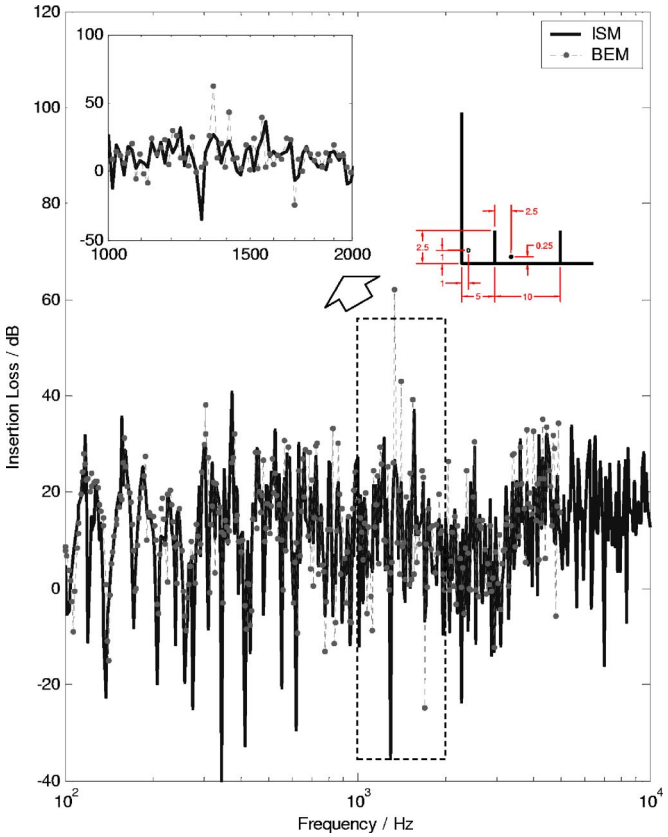

FIG. 5. (Color online) The spectrum of insertion losses at location $\mathfrak{R}=(1,0,1)$, with parallel barriers placed in front of a building façade. The solid line represents predictions by the image source method (ISM), and the dashed line with dots represents numerical predictions based on the boundary element method (BEM).

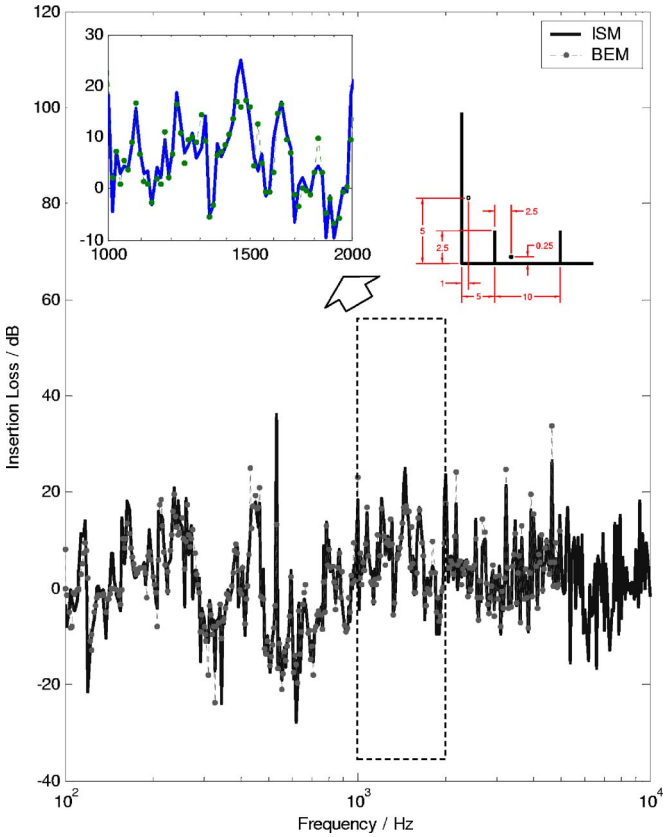

FIG. 6. (Color online) Same caption as Fig. 5 except that the receiver is located at $\mathfrak{R}=(1,0,5)$.

tions of the boundary surfaces. The levels of variation in *IL* reflect the phenomenon of interference due to the contributions from different image sources which is more pronounced at higher frequencies.

Figures 7 and 8 show the corresponding predicted results for the case of the street canyon with the receiver at Locations 2 and 4. The sound fields predicted by the image source method agree reasonably well with those predicted by the BEM formulation. The trends of the peak and dip of the *IL* spectrum predicted by the image source method are generally in agreement with those predicted by the BEM formulation. Again, considerable discrepancies are observed in predicting the magnitudes of *IL* by using the two different numerical methods. In comparison with the cases with a single façade, large fluctuations are observed in the insertion loss due to another set of image sources formed by placing a façade on the other side of the parallel barriers.

The *IL* spectrum is dependent on the geometrical configurations of the problem such as the locations of the parallel barriers and the relative positions of the source and receiver. It is possible to show that similar results can be obtained when the source and receiver are located at other positions. These results are not given here but are shown elsewhere.[13]

IV. EXPERIMENTAL VALIDATIONS

A model pair of parallel noise barriers, which was placed either in front of a façade or in a street canyon, was built at a scale of one-tenth for the present experimental study. Measured data were obtained to validate the image source model. The experimental setup is shown in Fig. 9 which reflects comparable source/receiver configurations discussed in the last section. We note that the setup for the parallel barriers in a street canyon is not shown in Fig. 9. The façade and ground surfaces are made of 8.5-mm-thick wooden boards, which were varnished to prevent sound leakage. Prior measurements[13] were conducted to measure the acoustic characteristic of the varnished wooden boards. We found that they can generally be treated as a perfectly reflecting plane. The heights of the façade and the pair of barriers are 2.44 and 0.5 m, respectively. The pair of barriers consists of two 3-mm-thick aluminum plates with lengths of 4.5 m. They are placed parallel to each other at a distance of 0.75 and 1.5 m in front of the façade.

A Tannoy speaker mounted on a long brass pipe with length of 1.5 m and diameter of 25 mm is used to simulate an omni-directional point source. Preliminary measurements are conducted to examine the directional characteristic of the point source. The measured result, not shown here for brevity, suggests that the deviation in the directivity pattern for all directions is within 1 dB for all frequencies above 250 Hz. Hence, the Tannoy sound source was placed parallel to the barriers as the most significant contributions were expected to be due to the reflections from the boundary surfaces.

In all measurements, the point source was located 1.25 m in front of the façade surface and at a height of 0.125

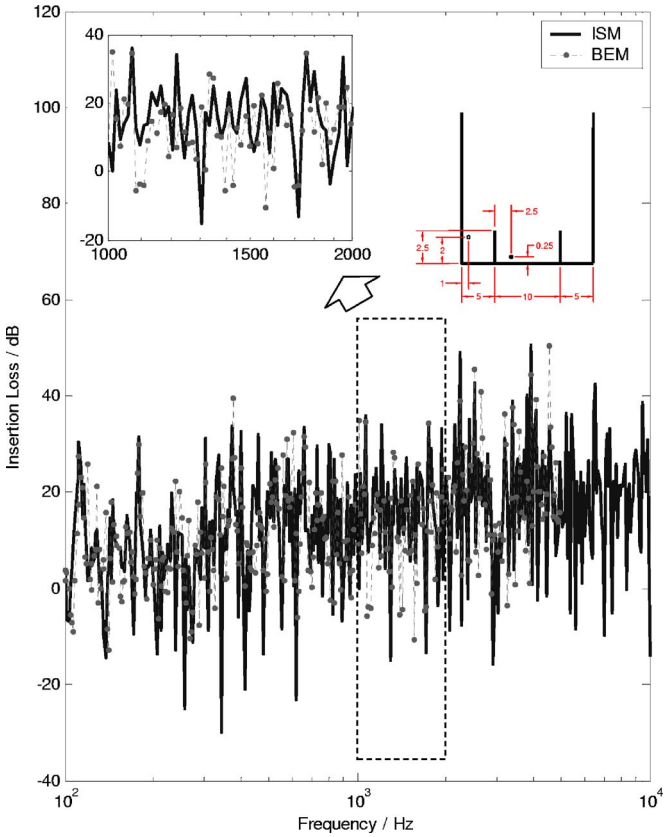

FIG. 7. (Color online) The spectrum of insertion losses (IL) at location $\mathfrak{R}=(1,0,2)$ with parallel barriers placed in a street canyon. The solid line represents predictions by the image source method (ISM) and the dashed line with dots represents numerical predictions based on the boundary element method (BEM).

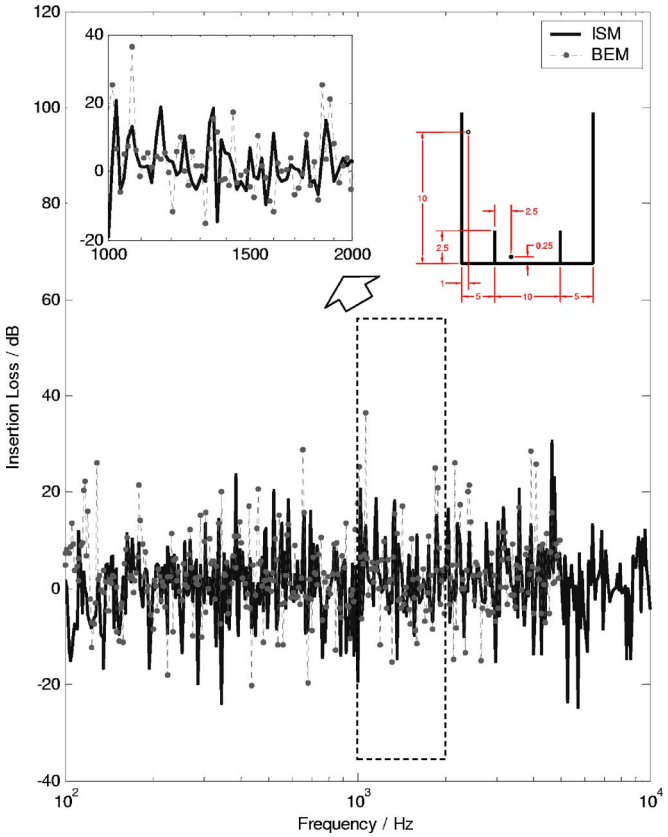

FIG. 8. (Color online) Same caption as Fig. 7 except that the receiver is located at $\mathfrak{R}=(1,0,10)$.

m above the ground. A B&K 4942 microphone, which was connected to a B&K 2671 preamplifier and a B&K NEXUS conditional amplifier, was used as the receiver. The microphone was placed at 0.123 m in front of the vertical wooden boards at various heights.

A special type of test signal called a maximum-length sequence (MLS) was employed to obtain the experimental data. The deterministic nature of the maximum-length sequence provides an excellent signal-to-noise ratio, which is ideal for the current indoor measurements. The MLS signals were generated by the MLSSA 2000 card, transferred via the built-in digital-to-analog-converter and boosted by a B&K 2713 power amplifier. The MLS signals were then connected to the Tannoy speaker, which emitted sound for measurements. As the measurements were recorded in the time domain, manipulation to eliminate unwanted reflections was also possible.

The experiments were conducted inside an anechoic chamber of dimensions 6 m $\times$ 6 m $\times$ 4 m (high). The insertion loss used for comparison was obtained by measuring the transfer function with and without the barrier. In the experimental measurements for the two cases described in Sec. II, the receiver was placed at four locations, A, B, C and D, at (0.123, 0, 0.1), (0.123, 0, 0.5), (0.123, 0, 1) and (0.123, 0, 1.5), respectively. Again, like the numerical validations, Locations A and B were situated in the shadow zone. Location C was placed in the penumbra region along the sight-line contact. Finally, Location D was chosen to be in the illumination region. We wish to point out that valid experimental data are not expected for frequencies below 500 Hz because of the size of the anechoic chamber and the scale model. Nevertheless, we show *IL* spectra with frequencies varying from 100 Hz to 10 kHz in the following plots.

Figures 10 and 11 illustrate the measured *IL* spectra at Locations B and D, respectively, for the model parallel barriers erecting in front of a building façade. Numerical simulations are also shown in these figures. For the narrow band spectra, measured data and numerical simulations show large fluctuations in the insertion loss spectra because of the complex interferences due to the contributions of different image

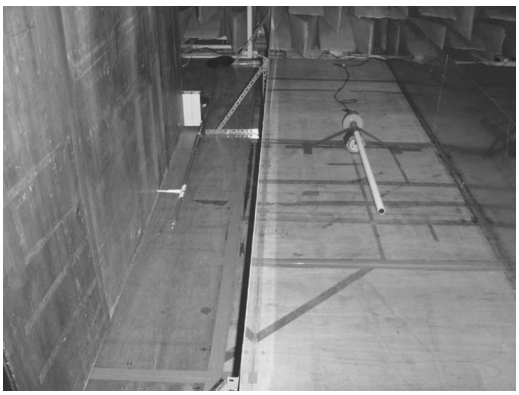

FIG. 9. The experimental setup for measurements in an anechoic chamber for a parallel barrier placed in front of a façade surface. The setup for a street canyon is not shown in the diagram.

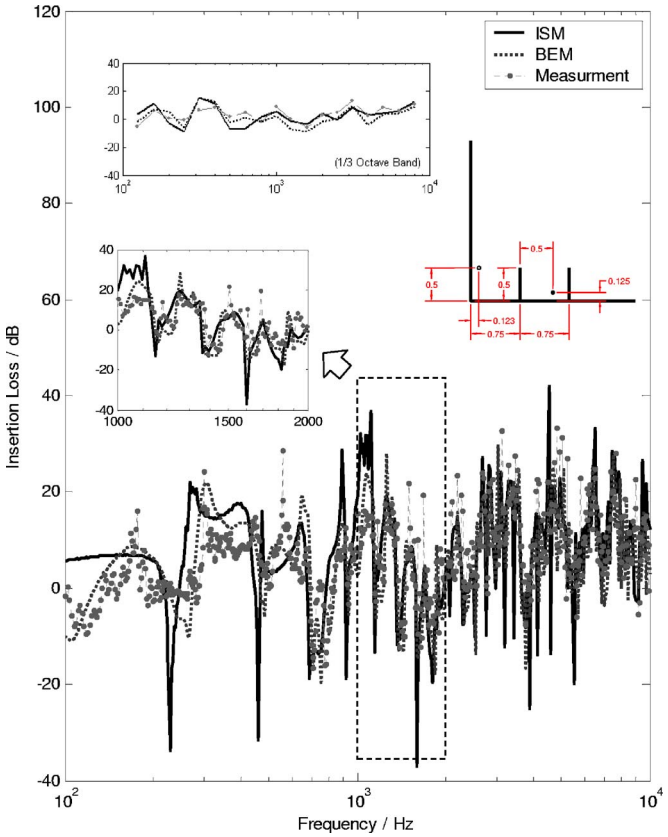

FIG. 10. (Color online) The spectrum of insertion losses at location $\mathfrak{R}=(0.123,0,0.5)$ with parallel barriers placed in front of a building façade. The solid line represents predictions by the image source method (ISM), the dashed line represents numerical predictions based on the boundary element method (BEM), and the dashed line with dots represents results from experimental measurement. Top inset figure: Comparison of the insertion loss between measured and predicted results in one-third octave band for a range of frequencies available from 125 to 8000 Hz. Bottom inset figure: Highlighting the narrow frequency spectrum going from 1000 to 2000 Hz.

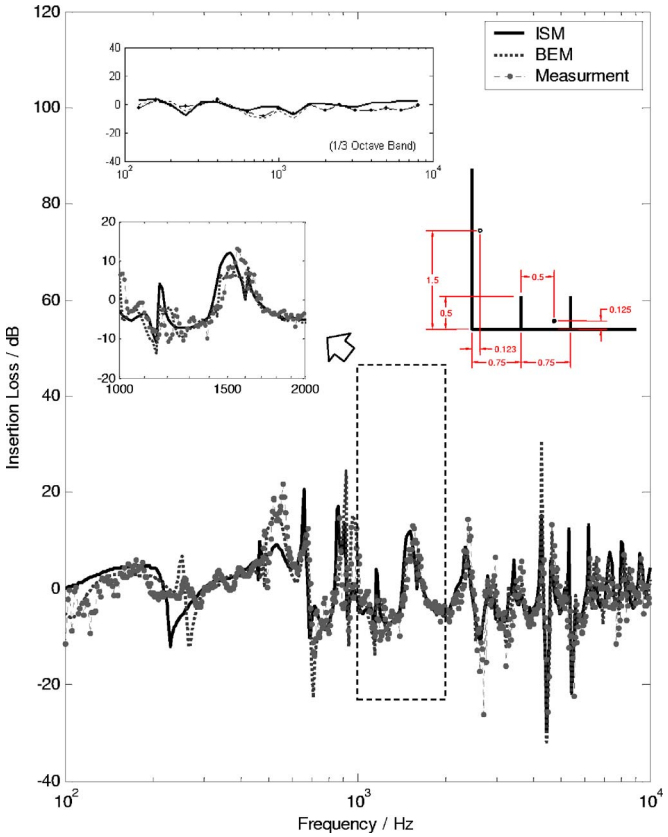

FIG. 11. (Color online) Same caption as Fig. 10 except that the receiver is located at $\mathfrak{R}=(0.123,0,1.5)$.

sources which have comparable magnitudes but with different phases. Numerical and experimental results of the frequency spectrum between 1000 and 2000 Hz are also shown in Fig. 10 in the inset figure. The constructive and destructive interferences of all rays are observed experimentally and they are predicted well by the image source model. This plot highlights the importance for including the information of the magnitudes and phases of each ray in the prediction model. The traditional energy-based ray model cannot be used to predict this wave interference effect.

In order to have a better quantitative comparison, the predictions and measurement of the insertion losses have also been compared in 1/3 octave bands for a range of frequencies varying from 125 to 8000 Hz as shown in the inset of Fig. 10. The predicted results (either by using the image source model or the BEM formulation) and measured data are generally in reasonably good agreement. Compared with the narrowband spectrum, the large fluctuations in the insertion loss are "smoothed" out in the 1/3 octave band spectrum.

Figure 11 shows the insertion loss for location D in which the receiver is located in the illumination region. In comparison with the previous case, the effect of interference is less observable for the frequency range of interest. It is because the receiver is located above the near side barrier which reduces the effect of multiple reflections between the boundary surfaces. Again, the inset figure shows good agreements in terms of constructive and destructive interferences between the measured results and the predictions according to the image source model for frequency ranging from 1000 to 2000 Hz. For the plot of the 1/3 octave bands, the image source model predicts very well the trend of the measured insertion loss.

Next, we show a comparison of the experimental results and theoretical predictions for the case of the parallel barriers placed in a street canyon. In Figs. 12 and 13, we display the comparisons of the experimental results and numerical predictions according to the image source model and BEM formulations at Locations A and C. There is an increase in the number of image sources in this experimental setup because of the presence of an additional building façade at the far side. This leads to an increase in the level of interference which can be observed in the measured data.

The overall compared results for this set of data are not as good as those shown earlier for the sound field of parallel placed in front a building façade. In this case, the finite size of building façades (both height and width) and the finite length of barriers play a significant role in the measured data. It is because extra diffractions at these edges, which have been ignored in the image source model, have comparable magnitudes to the higher-order reflected rays. Nevertheless, good agreements in terms of constructive and destructive interferences are evinced in Figs. 12 and 13 for both receiver

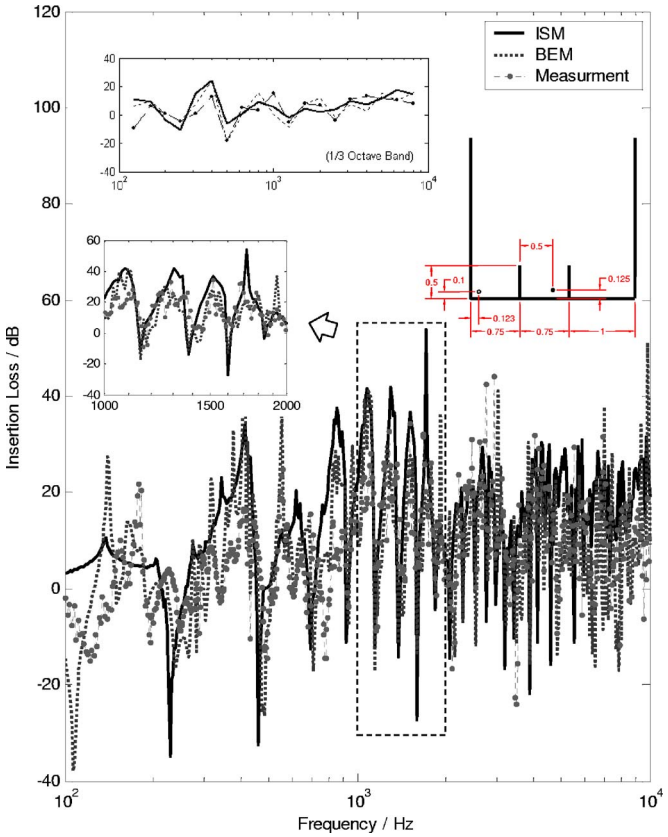

FIG. 12. (Color online) Same caption as Fig. 10 except that the receiver is located at $\mathfrak{R}=(0.123,0,0.1)$ and the parallel barriers are placed in a street canyon.

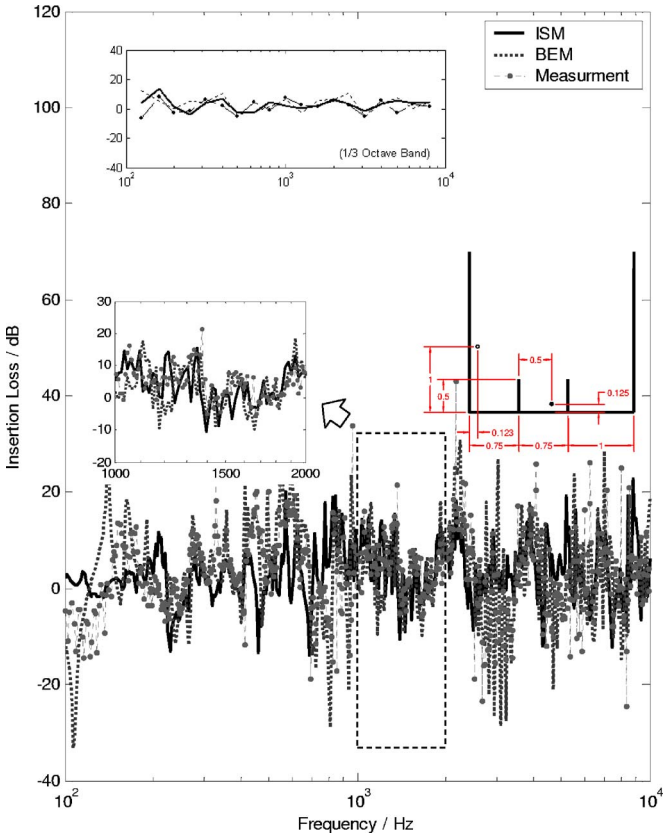

FIG. 13. (Color online) Same caption as Fig. 10 except that the receiver is located at $\mathfrak{R}=(0.123,0,1)$ and the parallel barriers are placed in a street canyon.

locations. Again, the large fluctuations in the sound fields are comparatively smoothed out for the data presented in the 1/3 octave bands. The image source model and BEM predictions are in accord with experimental measurements.

V. DISCUSSIONS AND CONCLUDING REMARKS

The development of a ray model for prediction of the performance of parallel barriers in high-rise cities is presented in this paper. Two typical cases in urban environments, (a) parallel barriers placed in front of a row of tall buildings and (b) parallel barriers in a street canyon, are considered. The contribution of the total sound field due to the effect of multiple reflections in parallel boundary surfaces is elucidated. The proposed ray model is validated by comparing it with indoor scale model experimental data and the BEM formulation, which is a more accurate but computationally intensive method. Compared with the BEM formulation, the ray model uses much fewer computational resources. Moreover, the ray model demonstrates its advantage in handling different frequencies simultaneously as long as all valid ray paths have been determined. This feature of handling different frequencies simultaneously is particularly useful for computing the 1/3 octave band noise levels. The ray model is a very useful numerical technique and computationally efficient in assessing the acoustic performance of parallel barriers in a high-rise city.

ACKNOWLEDGMENTS

This work was conducted while M.P.K. was a graduate student at the Hong Kong Polytechnic University. The research described in this paper was financed jointly by the Innovation and Technology Commission of the Hong Kong Special Administrative Region and the Mass Transition Railway Corporation Limited, through the award of an Innovation and Technology Fund under the category of the University-Industry Collaboration Program (Project No. UIM/39). The authors gratefully acknowledge the Research Committee of the Hong Kong Polytechnic University for the facilities and technical support provided throughout the period of the research. The authors thank Dr. Glenn H. Frommer of the MTR Corporation for his encouragement and many useful discussions.

[1]D. A. Hutchins and D. Pitcarn, "A laser study of multiple reflections within parallel barriers," J. Acoust. Soc. Am. **73**, 2216–2218 (1983).
[2]D. A. Hutchins and H. W. Jones, "Parallel barriers in the presence of ground surfaces," Noise Control Eng. J. **23**, 105–105 (1984).
[3]D. A. Hutchins, H. W. Jones, B. Paterson, and L. T. Russell, "Studies of parallel performance by acoustical modeling," J. Acoust. Soc. Am. **77**, 536–546 (1985).
[4]C. H. Chew, "Prediction of traffic noise from expressways – Part II: Building flanking both sides of expressways," Appl. Acoust. **32**, 61–72 (1991).
[5]Y. Sakurai, E. Walerian, and H. Morimoto, "Noise barrier for a building façade," J. Acoust. Soc. Jpn. **11**, 257–265 (1990).
[6]W. F. Cheng and C. F. Ng, "The acoustic performance of an inclined barrier for high-rise residents," J. Sound Vib. **242**, 295–308 (2001).
[7]L. Godinho, J. Antonio, and A. Tadeu, "3D sound scattering by rigid barriers in the vicinity of tall buildings," Appl. Acoust. **62**, 1229–1248

(2001).
[8]K. M. Li and S. H. Tang, "The predicted barrier effects in the proximity of tall buildings," J. Acoust. Soc. Am. **114**, 821–832 (2003).
[9]R. Panneton, A. L'Espérance, and G. A. Daigle, "Development and validation of a model predicting the performance of hard or absorbent parallel noise barriers," J. Acoust. Soc. Jpn. **14**, 251–258 (1993).
[10]A. Muradali and K. R. Fyfe, "A study of 2D and 3D barrier insertion loss using improved diffraction-based methods," Appl. Acoust. **53**, 49–75 (1998).
[11]W. J. Hadden and A. D. Pierce, "Diffraction of sound around corners and over wide barriers," J. Acoust. Soc. Am. **69**, 1266–1276 (1981).
[12]M. Abramowitz and A. Stegun, *Handbook of Mathematical Functions with Formulas, Graphs, and Mathematical Tables* (Dover, New York, 1970), Chap. 7, p. 300.
[13]M. P. Kwok, "Noise barriers in a complex urban environment," M. Phil. Thesis, The Hong Kong Polytechnic University, 2006.